

## Modeling and Current Control Strategy for a Medium-voltage Cascaded Multilevel STATCOM with LCL Filter

Xuehua Zhao<sup>\*,a</sup>, Liping Shi<sup>a</sup>, Libing Chen<sup>a</sup>, Zhenglong Xia<sup>b</sup>, A. R. Bendre<sup>c</sup>

<sup>a</sup>*School of Information & Electrical Engineering, China University of Mining & Technology  
Xuzhou, 221116, China*

<sup>b</sup>*School of Electrical Engineering, Jiangsu Normal University  
Xuzhou, 221000, China*

<sup>c</sup>*Faculty of Engineering, University of Wollongong  
Wollongong NSW, 2522, Australia*

### Abstract

The Static Synchronous Compensator (STATCOM a.k.a. SVG) is widely used to regulate dynamic reactive power and to solve dynamic voltage stability problems. Modeling shows that a cascaded STATCOM, which is composed of several cascaded H-bridges, not only has strong coupling characteristics when an LCL filter is added but it is also a non-linear, multivariable system. Therefore, its practical design and application are difficult to implement. In this paper an internal decoupling control algorithm is introduced to provide independent control of the active and reactive currents. Decoupling control algorithms are proposed, and models and simulation of the decoupling are provided. We describe the setting up of a simulation and experiments with a cascaded STATCOM based on combined circuit topology with a multi-field programmable gate array (FPGA), and double-loop control algorithms with a current inner loop, and a capacitor voltage outer loop. To provide control of the current inner loop, proportional-integral (PI) and resonant controllers are used, having the control ability to cancel harmonics while compensating for the reactive power. This paper presents new current-tracing control models that compensate for the fundamental current and eliminate selective harmonics by adopting a d-q synchronous reference frame, and a discrete Fourier transform (DFT). Voltage balance is realized by introducing modulation wave distribution strategies. Furthermore, both simulation and experiments are employed to verify the feasibility and effectiveness of the control strategy.

**Keywords:** Cascaded H-bridge, Internal model decoupling, Resonant controller, Distribution of modulation, Double-loop control

### 1. Introduction

The Static Synchronous Compensator (STATCOM) is one of the latest technologies in the field of reactive compensation, and is an important element of flexible alternating current transmission systems (FACTS). The STATCOM is connected in parallel to a power grid, allowing the compensator to be used as a controllable reactive current source as its reactive current quickly follows the changes of the load reactive current. The STATCOM automatically

provides dynamic reactive power compensation according to the reactive power needed in the power grid system. Conventional reactive power compensation devices, such as parallel capacitors, do not have fast, dynamic, smooth and continuous compensation characteristics, and cannot conform to the system requirements because of their poor dynamic regulation performance. The Static Var Compensator (SVC) is currently widely used as an important type of reactive power compensation device. However, if the reactive power of the system output decreases, the compensation effect becomes less than ideal if the output current reaches the maximum capacity of the SVC. There-

\*Corresponding author

Email address: cumtzh2013@126.com (Xuehua Zhao\*)

fore, medium-voltage cascaded STATCOMs have become the focus of research in recent years in an effort to provide effective regulation of power quality. The cascaded STATCOM with an H-bridge structure has obvious advantages relative to the multiple structures of traditional transformers. These advantages, apart from avoiding the need for multiple transformers, include high efficiency, scalability, and a modular design [1–3].

The H-bridges are multiple power units within each stage of the cascaded STATCOM. The output current of the STATCOM is optimized in terms of a rational parameter setup for LCL filter. Mathematical model analysis shows that a cascaded STATCOM, which is constructed from several cascaded H-bridges, is a non-linear, multi-variable, strongly coupled system. These properties cause difficulties in the design and practical application of the controller [4–8].

Mathematical models, which use the d- and q-axis system currents as state control variables, can be deduced in the a-b-c and d-q coordinates through equivalent conversion and simplification. The active component of the load current need not be considered when analyzing the system current. Using internal model control theory and proportional-integral (PI) control strategies as a basis, an internal decoupling control algorithm can be employed to provide independent control of the active and reactive currents. The research reported herein introduces the idea of double-loop control algorithms, with a current inner loop and capacitor voltage outer loop, allied with a multi-Field Programmable Gate Array (FPGA) structure. These algorithms compensate for the fundamental current and eliminate the 5th and 7th, 11th and 13th, and 17th and 19th harmonics by adopting selective harmonic technology. This paper applies a d-q synchronous reference frame and discrete Fourier transform (DFT) to simplify the control principle and reduce the number of controllers. Accordingly, the system only needs to complete the compensation of the fundamental current and the 6th, 12th, and 18th harmonics by adopting proportional-integral (PI) and resonant controller technology [9–11].

An adaptive dynamic layered control scheme, taking account of the balance control of the total DC capacitor voltage, the phase-to-phase voltage, and the voltage between each unit, is proposed in the control process because of the voltage imbalance issue in the voltage outer loop. This paper also proposes another control method, using modulation wave distribution strategies, to allocate the switch action of the H-bridges for maintaining the voltage balance [12–15].

We established our simulation models and the experi-

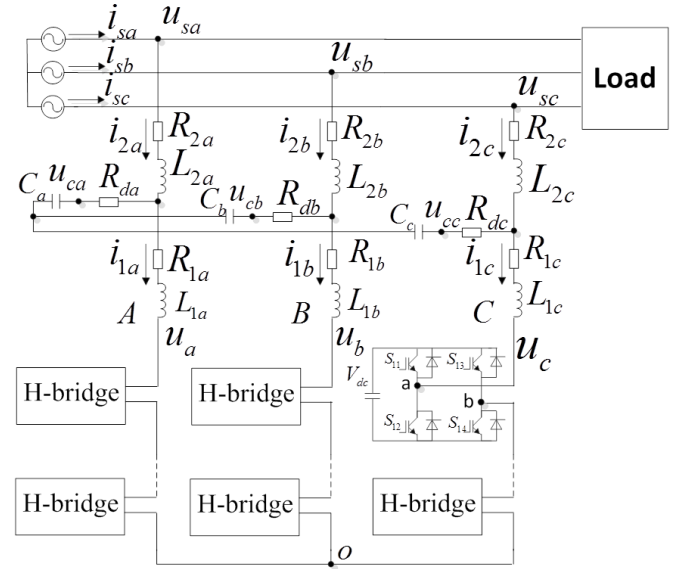


Figure 1: Main circuit model for a cascaded STATCOM

mental techniques used to verify the rationality of the system structure and control strategies based on our research into the development background of medium-voltage cascaded STATCOMs. The performance in both dynamic and steady-state situations is analyzed in our simulations and by experiment. The simulation and experimental results show that the proposed mathematical models and strategies are feasible and effective, and, moreover, that the control of the reactive current of the STATCOM has a rapid dynamic response and good stability characteristics.

## 2. Topological structure and model analysis

### 2.1. Main circuit structure

The main circuit model of a medium-voltage cascaded STATCOM is shown in Fig. 1.  $u_{sa}$ ,  $u_{sb}$  and  $u_{sc}$  denote the three-phase voltage of the power grid;  $i_{sa}$ ,  $i_{sb}$  and  $i_{sc}$  indicate the three-phase current of the power grid;  $i_{La}$ ,  $i_{Lb}$  and  $i_{Lc}$  represent the three-phase current of the load;  $i_{2a}$ ,  $i_{2b}$  and  $i_{2c}$  denote the three-phase output current of the filter;  $i_{1a}$ ,  $i_{1b}$  and  $i_{1c}$  indicate the three-phase output current of the STATCOM;  $u_a$ ,  $u_b$  and  $u_c$  represent the three-phase output voltage of the STATCOM.

Each phase of the medium-voltage cascaded STATCOM comprises eight H-bridge cells to form the cascaded structure. The distributed H-bridges are the main power devices used to form the three-phase system of the STATCOM, while the wiring adopts a star connection method. An LCL filter is adopted to provide optimized control of

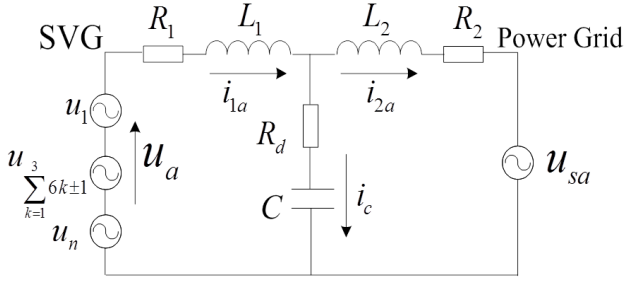


Figure 2: Single-phase equivalent model of a STATCOM with LCL filter

the output current in order to reduce the current harmonics around the switching frequency of the three-phase pulse width modulation (PWM) rectifiers. The power exchange between the grid and the STATCOM is achieved by changing the size and phase of the output voltage. The measured voltage and current signals are accessed in the main controller to generate the trigger signals.

## 2.2. Mathematical model of a STATCOM using the output current as state variable

A single-phase equivalent model can be created, based on the main circuit model of the medium-voltage cascaded STATCOM. This model is shown in Fig. 2.

If the STATCOM output current, capacitance voltage and filter output currents  $i_1$ ,  $u_c$  and  $i_2$  are taken as the state variables, a state equation can be established on the basis of the single-phase equivalent model and the d-q synchronous reference frame.

$$\begin{cases} \frac{di_{1d}}{dt} = -\frac{R_1}{L_1}i_{1d} + \omega i_{1q} - \frac{1}{L_1}u_{cd} + \frac{1}{L_1}u_d \\ \frac{di_{1q}}{dt} = -\frac{R_1}{L_1}i_{1q} - \omega i_{1d} - \frac{1}{L_1}u_{cq} + \frac{1}{L_1}u_q \\ \frac{di_{2d}}{dt} = -\frac{R_2}{L_2}i_{2d} + \omega i_{2q} + \frac{1}{L_2}u_{cd} - \frac{1}{L_2}u_d \\ \frac{di_{2q}}{dt} = -\frac{R_2}{L_2}i_{2q} - \omega i_{2d} + \frac{1}{L_2}u_{cq} - \frac{1}{L_2}u_q \\ \frac{du_{cd}}{dt} = \frac{1}{C}(i_{1d} - i_{2d}) + \omega u_{cq} \\ \frac{du_{cq}}{dt} = \frac{1}{C}(i_{1q} - i_{2q}) - \omega u_{cd} \end{cases} \quad (1)$$

The reactive and active components  $u_d$  and  $u_q$  in the d-q synchronous reference frame are used to express the output current of the STATCOM. The voltage variables  $u_d$  and  $u_q$  are the d- and q-axis current components of the power grid.

The preceding formula indicates that the output current components of the STATCOM in the d-q coordinate depend not only on the coupled voltages (i.e.,  $\omega L_1 i_{1q}$ ,  $-\omega L_1 i_{1d}$ ,  $\omega L_2 i_{2q}$  and  $-\omega L_2 i_{2d}$ ) and the coupled currents (i.e.,  $\omega C u_{cq}$  and  $-\omega C u_{cd}$ ) but also on the voltage of the power grid (i.e.,  $u_{sd}/u_{sq}$ ). Therefore, designing a decoupling control

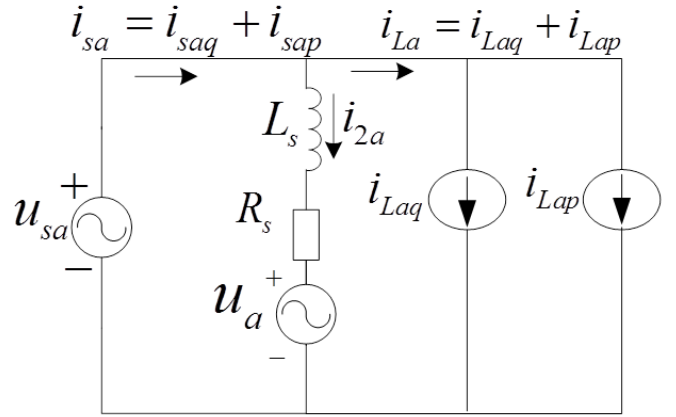


Figure 4: Single phase equivalent model

scheme with a closed loop control is necessary in order to obtain the expected control performance for current control instruction (i.e.  $u_d$  and  $u_q$ ).

The voltage components of the STATCOM in the d-q coordinates are expressed as Eq. (2), using the state feedback decoupling control. The principle diagram, based on such state feedback decoupling control is shown in Fig. 3.

$$\begin{cases} u_d = u_{d1} - \omega L_1 i_{1q} - \omega C(L_1 s + R_1)u_{cq} \\ \quad - \omega L_2(L_1 s + R_1)C s i_{2q} \\ u_q = u_{q1} - \omega L_1 i_{1d} - \omega C(L_1 s + R_1)u_{cd} \\ \quad - \omega L_2(L_1 s + R_1)C s i_{2d} \end{cases} \quad (2)$$

Problems may arise if such a decoupling control approach, based on the introduction of state feedback variables, is used for the coupling variables. (i.e.,  $i_{2d}$ ,  $i_{2q}$ ,  $u_{cd}$  and  $u_{cq}$ ). These issues may include the introduction of too many state variables to readily solve the resulting group of complex differential equations. Importantly, the accuracy of the controller will clearly be dependent upon the number and precision of the control parameters.

## 2.3. Simplified model of cascaded STATCOM in the a-b-c coordinates

The preceding analysis demonstrates that a cascaded STATCOM is a non-linear, multivariable, strongly coupled system which can therefore result in a certain degree of difficulty related to control. The cascaded STATCOM uses LCL filters, their main purpose being to filter the output harmonic components. System analysis can simplify the LCL filter structure to represent it as an L filter.  $L_s$  and  $R_s$  are defined as the inductance and resistance of the L filter. The three phase models are independent of, but

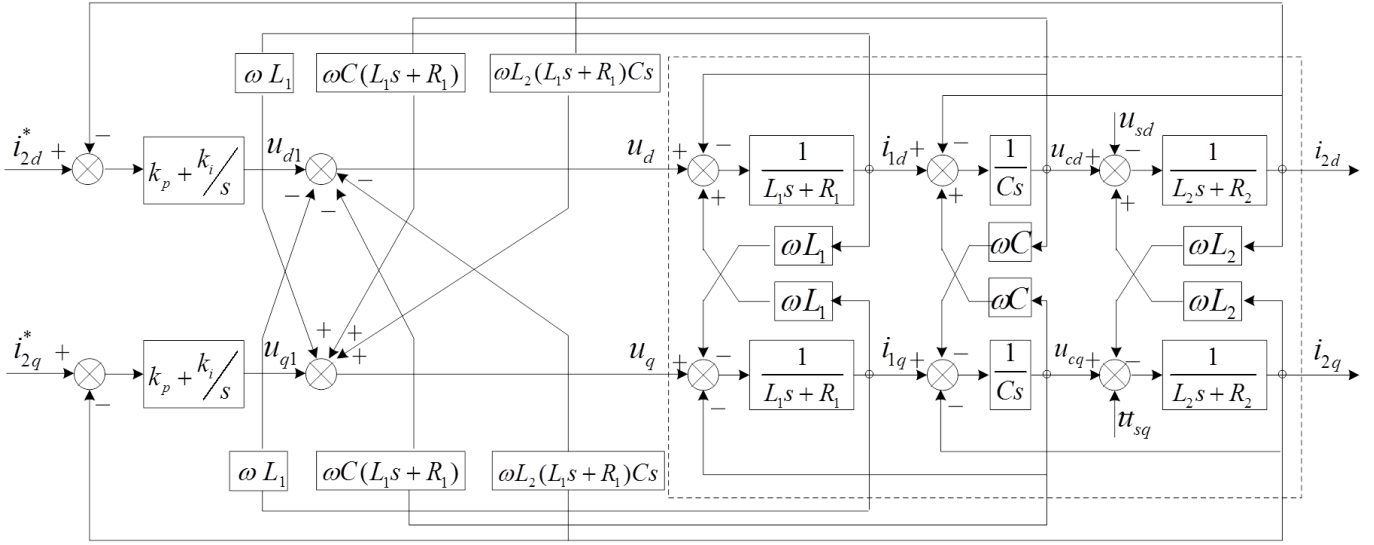


Figure 3: Principle diagram based on feedback decoupling control

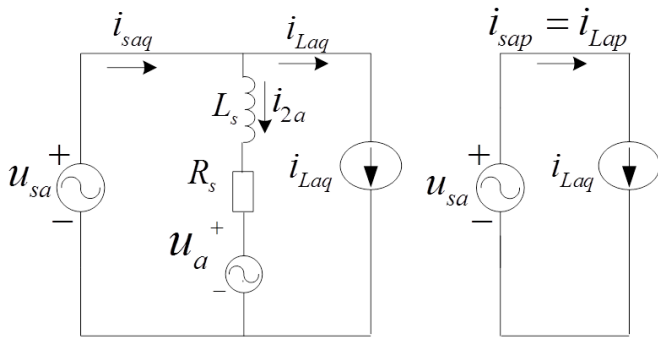


Figure 5: Equivalent model of compensation

symmetrical to each other. Therefore, an A-phase system current is typically chosen as the research object. The established single-phase equivalent circuit model is shown in Fig. 4. The variables (i.e.,  $i_{saq}$ ,  $i_{sap}$ ,  $i_{Laq}$  and  $i_{Lap}$ ) represent the system reactive and active currents and the load reactive and active currents of the A-phase model, respectively. The system and load currents are expressed as follows:

$$\begin{cases} i_{sa} = i_{saq} + i_{sap} \\ i_{La} = i_{Laq} + i_{Lap} \end{cases}$$

The single-phase equivalent circuit model of the A-phase can be considered as two separate circuits. The specific model is shown in Fig. 5. The active and reactive currents in the circuits are controlled independently with a compensation device aiming to provide the reactive component. The reactive current, before compensa-

tion, can be represented as follows, with the power grid providing the reactive current.

$$\begin{cases} i_{sa} = i_{La} \\ i_{sap} = i_{Lap} \\ i_{saq} = i_{Laq} \end{cases} \quad (3)$$

The reactive components of the system current, device current, and load current, after compensation, should satisfy the following condition, with the compensation device providing all of the reactive current for the load.

$$\begin{cases} i_{2a} = i_{Laq} \\ i_{sap} = i_{Lap} \\ i_{saq} = 0 \end{cases} \quad (4)$$

The A-phase equivalent model of the cascaded STATCOM in Fig. 5 is expressed as follows:

$$u_{sa}(t) = L_s \frac{d(i_{saq}(t) - i_{Laq}(t))}{dt} + R_s(i_{saq}(t) - i_{Laq}(t)) + u_a(t) \quad (5)$$

that is,

$$\frac{di_{saq}(t)}{dt} = \frac{di_{Laq}(t)}{dt} - \frac{R_s i_{saq}(t)}{L_s} + \frac{R_s i_{Laq}(t)}{L_s} + \frac{u_{sa}(t)}{L_s} - \frac{u_a(t)}{L_s} \quad (6)$$

Similarly, the equivalent mathematical models of the B- and C-phases are respectively built as follows:

$$\frac{di_{sbq}(t)}{dt} = \frac{di_{Lbq}(t)}{dt} - \frac{R_s i_{sbq}(t)}{L_s} + \frac{R_s i_{Lbq}(t)}{L_s} + \frac{u_{sb}(t)}{L_s} - \frac{u_b(t)}{L_s} \quad (7)$$

$$\frac{di_{scq}(t)}{dt} = \frac{di_{Lcq}(t)}{dt} - \frac{R_s i_{scq}(t)}{L_s} + \frac{R_s i_{Lcq}(t)}{L_s} + \frac{u_{sc}(t)}{L_s} - \frac{u_c(t)}{L_s} \quad (8)$$

The mathematical models of the cascaded STATCOM in the a-b-c coordinates are presented in Eqs (6)–(8).

Subsequently, Eqs. (6)–(8) are simplified as follows, if the preceding equations meet the following conditions,  $i_{sabcq} = \langle i_{saq}, i_{sbq}, i_{scq} \rangle$ ,  $u_{sabc} = \langle u_{sa}, u_{sb}, u_{sc} \rangle$ ,  $i_{Labcq} = \langle i_{Laq}, i_{Lbq}, i_{Lcq} \rangle$ , and  $u_{abc} = \langle u_a, u_b, u_c \rangle$ :

$$\frac{di_{sabcq}(t)}{dt} = \frac{di_{Labcq}(t)}{dt} - \frac{R_s i_{sabcq}(t)}{L_s} + \frac{R_s i_{Labcq}(t)}{L_s} + \frac{u_{sabc}(t)}{L_s} - \frac{u_{abc}(t)}{L_s} \quad (9)$$

#### 2.4. Modeling of cascaded STATCOM based on the d-q synchronous reference frame

An analysis of the preceding equations shows that the cascaded STATCOM models in the a-b-c coordinates are differential equations with time-variable coefficients. This condition makes theoretical analysis difficult. A d-q synchronous reference frame can be used to simplify the dynamic models. The relationship of the three-phase coordinate transformation matrix (i.e., Park transform) is presented as follows:

$$T = \sqrt{\frac{2}{3}} \begin{bmatrix} \sin \omega t & \sin(\omega t - \frac{2}{3}\pi) & \sin(\omega t + \frac{2}{3}\pi) \\ \cos \omega t & \cos(\omega t - \frac{2}{3}\pi) & \cos(\omega t + \frac{2}{3}\pi) \end{bmatrix} \quad (10)$$

The parameter (i.e.,  $\omega = 2\pi f$ ) in Eq. (10) denotes the angular frequency of the fundamental current. The relationship of the three-phase coordinate transformation and the coordinate inverse transformation matrices between the a-b-c and d-q coordinates is illustrated as follows:

$$\begin{cases} x_{dq0} = T x_{abc} \\ x_{abc} = T^{-1} x_{dq0} \end{cases} \quad (11)$$

where  $x_{abc}$  and  $x_{dq0}$  are the corresponding vectors in the a-b-c and d-q coordinates, respectively.

The mathematical model of the cascaded STATCOM in the d-q coordinates can be simplified as follows, and the transfer relation of the variables should meet the following conditions:

$$i_{sabcq} = \langle i_{sqd}, i_{sqq} \rangle, u_{sabc} = \langle u_{sd}, u_{sq} \rangle, i_{Labcq} = \langle i_{Lqd}, i_{Lqq} \rangle, \text{ and } u_{abc} = \langle u_d, u_q \rangle:$$

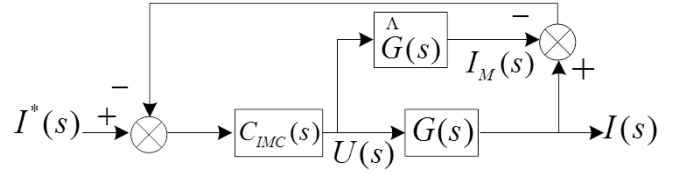


Figure 6: Principle block diagram of IMC

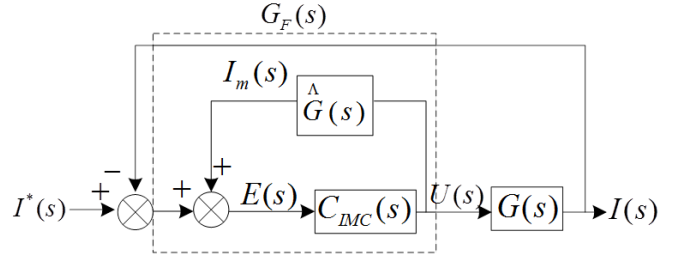


Figure 7: Equivalent feedback control principle diagram

$$\begin{bmatrix} \frac{di_{sqd}}{dt} \\ \frac{di_{sqq}}{dt} \end{bmatrix} = \begin{bmatrix} -\frac{R_s}{L_s} i_{sqd} + \omega i_{sqq} + \frac{1}{L_s} u_{sd} + \frac{di_{Lqd}}{dt} + \frac{R_s}{L_s} i_{Lqd} - \omega i_{Lqq} - \frac{1}{L_s} u_d \\ -\frac{R_s}{L_s} i_{sqq} - \omega i_{sqd} + \frac{1}{L_s} u_{sq} + \frac{di_{Lqq}}{dt} + \frac{R_s}{L_s} i_{Lqq} + \omega i_{Lqd} - \frac{1}{L_s} u_q \end{bmatrix} \quad (12)$$

where the output variables (i.e.,  $u_d$  and  $u_q$ ) of the STATCOM are used as the input variables, and the system current variables (i.e.,  $i_{sqd}$  and  $i_{sqq}$ ) are utilized as the control variables.

The model shows that coupling relationships also exist between the reactive and active currents. Hence, a decoupling control algorithm is required to provide independent control of the active and reactive currents.

### 3. Current decoupling design based on internal model control (IMC)

#### 3.1. Principle of internal model control

The principle diagram of the internal model control is shown in Fig. 6.

Accordingly,  $\hat{G}(s)$  is the internal control model;  $G(s)$  represents the controlled objects; and  $G_{IMC}(s)$  is the internal model controller. The equivalent feedback control principle diagram for the internal model of control is shown in Fig. 7. The equivalent controller is expressed as follows:

$$G_F(s) = [I - C_{IMC}(s) \hat{G}(s)]^{-1} C_{IMC}(s) \quad (13)$$

### 3.2. Decoupling control strategy based on the internal model

The state equations of Eq. (12) are expressed as follows using the Laplace transform method:

$$\begin{cases} u_d - u_{sd} - sL_s i_{Lqd} - R_s i_{Lqd} + L_s \omega i_{Lqq} \\ u_q - u_{sq} - sL_s i_{Lqq} - R_s i_{Lqq} + L_s \omega i_{Lqd} \end{cases} \quad (14)$$

$$= \begin{bmatrix} sL_s + R_s & -L_s \omega \\ L_s \omega & sL_s + R_s \end{bmatrix} \begin{bmatrix} i_{sqd} \\ i_{sqq} \end{bmatrix}$$

Consequently, if the preceding equations meet the following two conditions,

$$\begin{cases} v_d = u_d - u_{sd} - sL_s i_{Lqd} - R_s i_{Lqd} + L_s \omega i_{Lqq} \\ v_q = u_q - u_{sq} - sL_s i_{Lqq} - R_s i_{Lqq} + L_s \omega i_{Lqd} \end{cases} \quad (15)$$

Eq. (14) can be simplified as follows:

$$\begin{bmatrix} v_d \\ v_q \end{bmatrix} = \begin{bmatrix} sL_s + R_s & -L_s \omega \\ L_s \omega & sL_s + R_s \end{bmatrix} \begin{bmatrix} i_{sqd} \\ i_{sqq} \end{bmatrix} \quad (16)$$

The derivation of  $\hat{G}^{-1}(s)$  and  $L(s)$  is presented in the following equations:

$$\hat{G}^{-1}(s) = \begin{bmatrix} sL_s + R_s & -L_s \omega \\ L_s \omega & sL_s + R_s \end{bmatrix};$$

$$L(s) = \begin{bmatrix} \lambda/(s + \lambda) & 0 \\ 0 & \lambda/(s + \lambda) \end{bmatrix}, \text{ then}$$

$$\begin{aligned} C_{IMC}(s) &= G^{-1} \wedge \cdot L(s) \\ &= \begin{bmatrix} sL_s + R_s & -L_s \omega \\ L_s \omega & sL_s + R_s \end{bmatrix} \begin{bmatrix} \lambda/(s + \lambda) & 0 \\ 0 & \lambda/(s + \lambda) \end{bmatrix} \\ &= \lambda \begin{bmatrix} \frac{sL_s + R_s}{s + \lambda} & \frac{-L_s \omega}{s + \lambda} \\ \frac{L_s \omega}{s + \lambda} & \frac{sL_s + R_s}{s + \lambda} \end{bmatrix} \end{aligned} \quad (17)$$

The result of the analysis indicates that the response characteristic when using a larger parameter value (i.e.,  $\lambda = 1/T$ ) has smaller inertia, quicker response and a larger overshoot, whereas a smaller parameter value reflects the opposite control effect. The input and output transfer functions can be deduced as follows, using the equivalent feedback control principle diagram for the internal model controller:

$$\frac{I(s)}{I^*(s)} = \frac{G_F(s)G(s)}{1 + G_F(s)G(s)} = \frac{C_{IMC}(s)G(s)}{1 + C_{IMC}(s)[G(s) - \hat{G}(s)]} \quad (18)$$

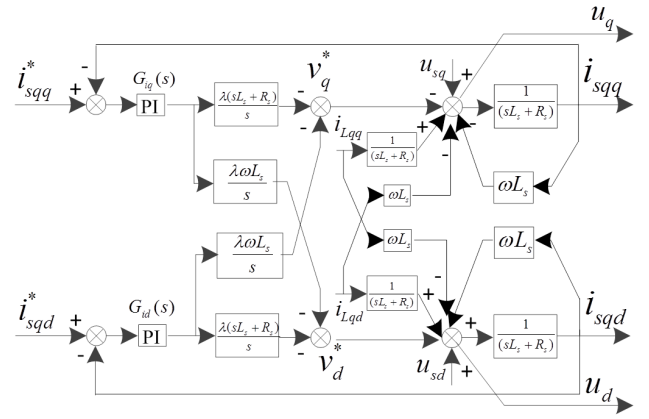


Figure 8: Decoupling diagram of internal model control

$$I(s) = \begin{bmatrix} i_{sqd} \\ i_{sqq} \end{bmatrix}, I^*(s) = \begin{bmatrix} i_{sqd}^* \\ i_{sqq}^* \end{bmatrix}, \text{ then}$$

$$\begin{aligned} G_F(s) &= [I - C_{IMC}(s)\hat{G}(s)]^{-1} C_{IMC}(s) \\ &= \left[ I - \frac{\lambda}{s + \lambda} I \right]^{-1} G^{-1}(s) \frac{\lambda}{s + \lambda} \\ &= \lambda \begin{bmatrix} \frac{sL_s + R_s}{s} & \frac{-L_s \omega}{s} \\ \frac{L_s \omega}{s} & \frac{sL_s + R_s}{s} \end{bmatrix} \end{aligned} \quad (19)$$

Subsequently, Eq. (18) is represented as Eq. (20) when the  $G(s) = \hat{G}(s)$  condition is true.

$$\frac{I(s)}{I^*(s)} = L(s) \quad (20)$$

If the algorithm plugs equation ( $I(s)$  and  $I^*(s)$ ) into (20), then the decoupling control algorithm is finally realized in Eq. (21).

$$\begin{bmatrix} i_{sqd} \\ i_{sqq} \end{bmatrix} = \begin{bmatrix} \lambda/(s + \lambda) & 0 \\ 0 & \lambda/(s + \lambda) \end{bmatrix} \begin{bmatrix} i_{sqd}^* \\ i_{sqq}^* \end{bmatrix} \quad (21)$$

The  $G(s) = \hat{G}(s)$  formula becomes true if the necessary parameters (i.e.,  $L_s$  and  $R_s$ ) are accurately designed. By contrast, the equivalent response of the system and its reference current (i.e.,  $I$  and  $I^*$ ) is assumed as an inertial link (i.e.,  $\lambda/s + \lambda = 1/1 + Ts$ ) by choosing the larger parameter's  $\lambda$  value. A proportional-integral (PI) controller is also introduced into the control algorithm to achieve an ideal response effect. The first-order internal model control principle block diagram of the STATCOM, following the decoupling control principle is shown in Fig. 8.

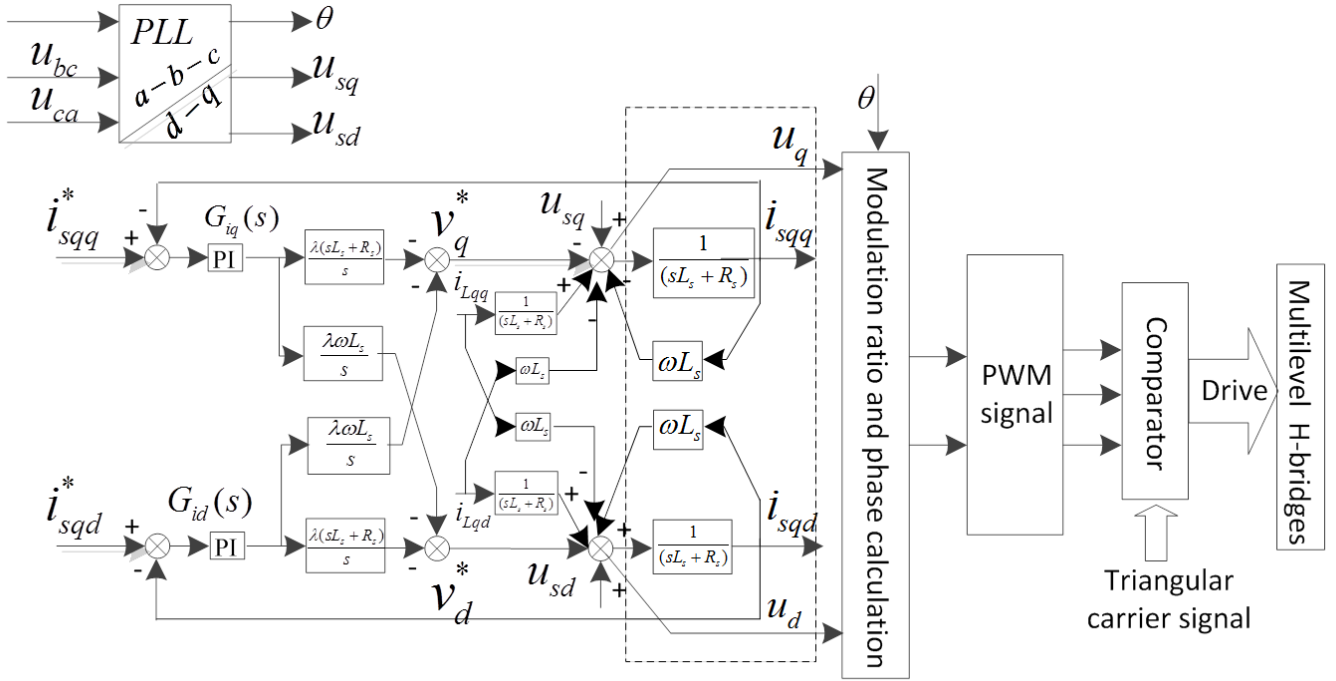


Figure 9: System simulation model

Table 1: Simulation Parameters

Parameters	Value
1 Voltage class	380 V
2 Capacity	$\pm 0.1$ M
3 Number of power units	3
4 DC-side capacitors	10 $\mu$ F
5 Filter reactor	2 mH 8.4 mH
6 Filter capacitor	6.76 $\mu$ F
7 Filter resistance	8.55 $\Omega$

## 4. Simulation and experiment

### 4.1. Simulation platform for the system

The simulation system was built using a mathematical model in the a-b-c and d-q-0 coordinates; and an internal model decoupling control algorithm was adopted to provide independent control of the active and reactive currents. The simulation model is shown in Fig. 9. The system simulation platform is based on the main circuit model of the STATCOM (Fig. 1). The simulation parameters are shown in Table 1.

The output variables (i.e.,  $u_d$  and  $u_q$ ) of the STATCOM in the preceding model are used as the input variables. The system current variables (i.e.,  $i_{sqd}$  and  $i_{sqq}$ ) are used as the control variables, and should satisfy the fol-

lowing condition:  $i_{sqd}^* = 0$  and  $i_{sqq}^* = 0$ . The reference voltages (i.e.,  $v_q^*$  and  $v_d^*$ ) are employed to achieve control of the output current, using the preceding decoupling method. The three-phase output voltage signals (i.e.,  $u_a$ ,  $u_b$  and  $u_c$ ), generated by the triangle carrier waves from subordinate controllers and modulation waves from the main controller, are used to drive the H-bridge circuits.

### 4.2. New current-tracing control model using DFT and d-q synchronous reference frame

The proportional-integral (PI) controller may not perform well in a situation where the reference signals (i.e.,  $i_d^*$  and  $i_q^*$ ) are AC signals. This study adopts resonance controllers to provide zero steady-state error control for the selected harmonic currents (i.e., the 5<sup>th</sup> and 7<sup>th</sup>, 11<sup>th</sup> and 13<sup>th</sup>, and 17<sup>th</sup> and 19<sup>th</sup> harmonic currents). The positive sequence part of the  $n$  order harmonic current in the a-b-c coordinates is then transformed into the  $(n - 1)$  order control component in the d-q coordinates. The  $(n + 1)$  order control part in the d-q coordinates is used to control the negative sequence part of the  $n$  order harmonic current in the a-b-c coordinates. The above result shows that the system only needs to complete compensation of the 6<sup>th</sup>, 12<sup>th</sup>, and 18<sup>th</sup> harmonic currents. The new detection and control model is shown in Fig. 10.

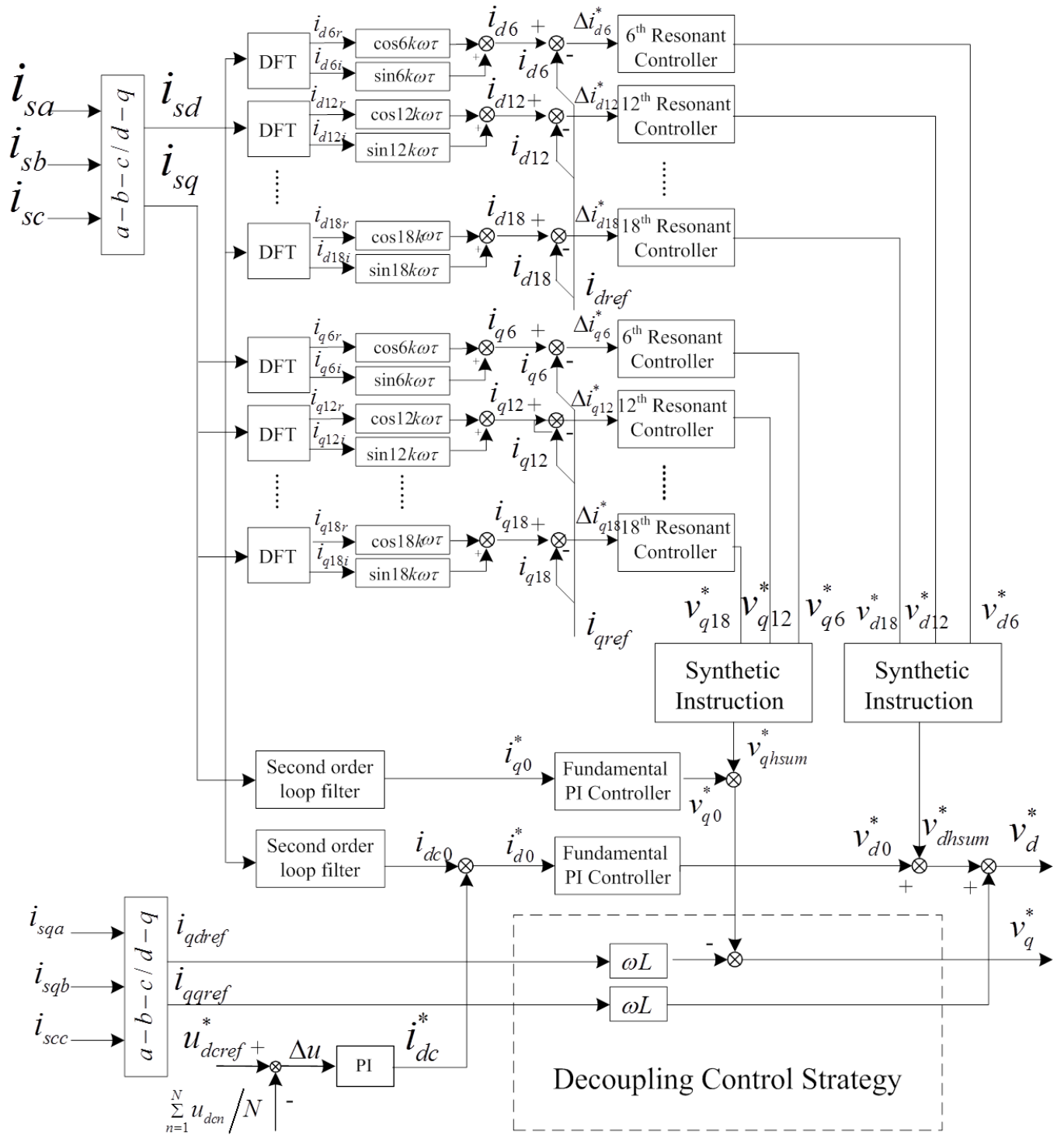


Figure 10: New current-tracing control model based on coordinates transform and DFT

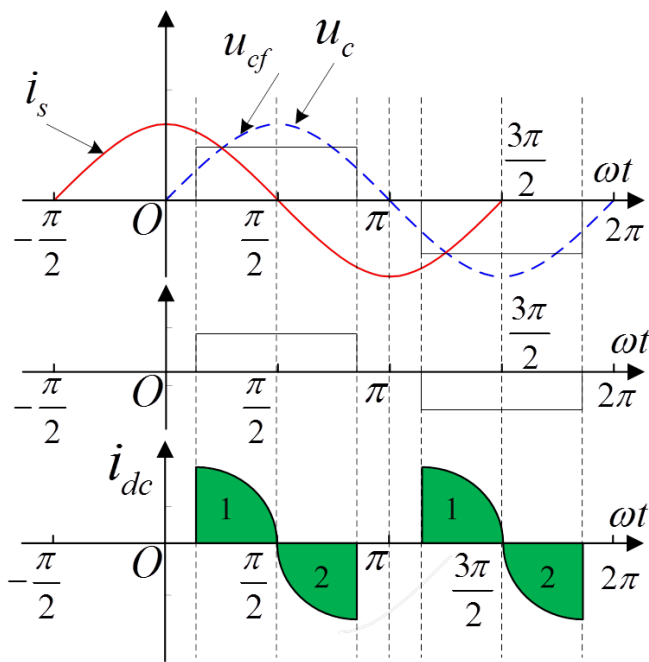


Figure 11: Energy balance principle of H-bridge

#### 4.3. Modulation Wave Distribution Strategies

Next we investigated the use of modulation wave distribution strategies in providing a voltage balance control scheme to solve the problem of the voltage imbalance of the DC-side capacitors. These strategies were then added to the adaptive dynamic layered control scheme to form the control strategies of the integrated voltage, the phase-to-phase voltage, and each unit voltage.

The energy balance principle of the H-bridge structure shows that the DC-side capacitors are always in a charging state in the negative half-cycle of the fundamental current (Fig. 11). By contrast, the capacitor releases energy, and the capacitor voltage drops in the positive half-cycle. Hence, this study used modulation wave distribution methods to solve the voltage imbalance problem of the DC-side capacitors by controlling the insulated-gate bipolar transistor (IGBT) switch frequency and the conducting time of the different H-bridges. The voltage comparison between the capacitors is conducted one time per control cycle. The specific allocation strategy is shown in Fig. 12.

#### 4.4. Verification of the cascaded STATCOM simulation in MATLAB

In order to simulate the actual project in various operating conditions, load simulation system uses capacitive and inductive loads in both cases. A harmonic source

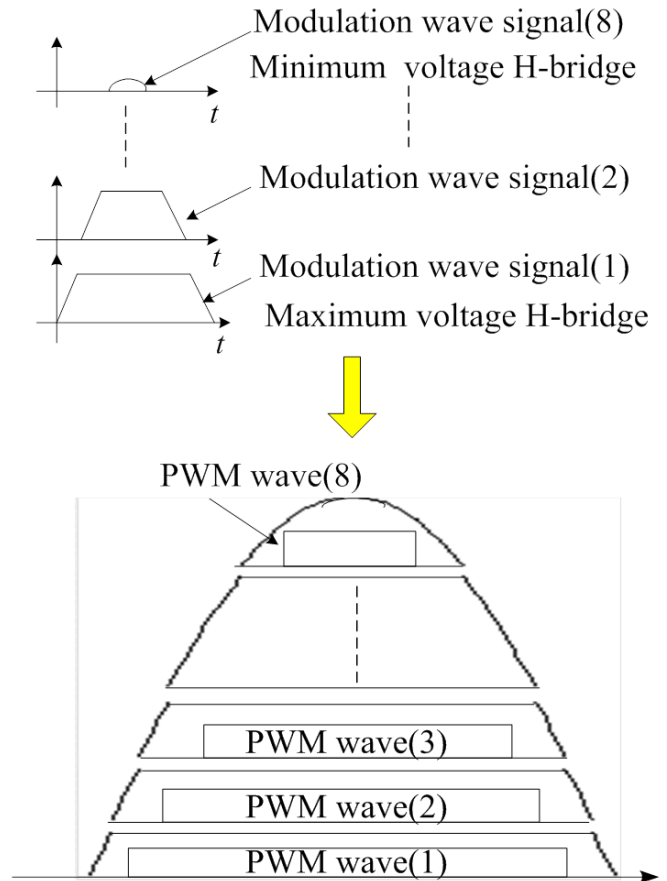


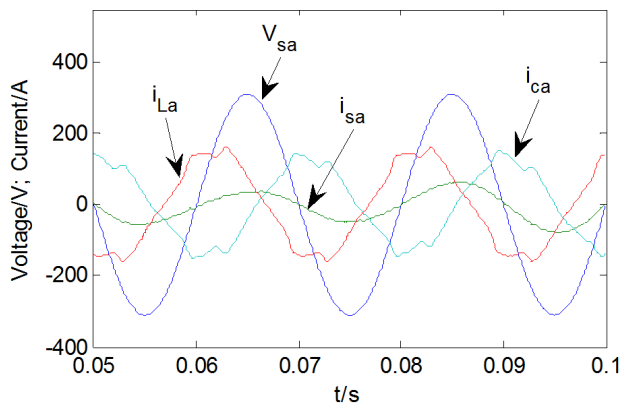
Figure 12: Modulation wave distribution strategies

model, which represents the universal bridges, the resistances, and the inductances, was used to simulate the harmonic components of the load.

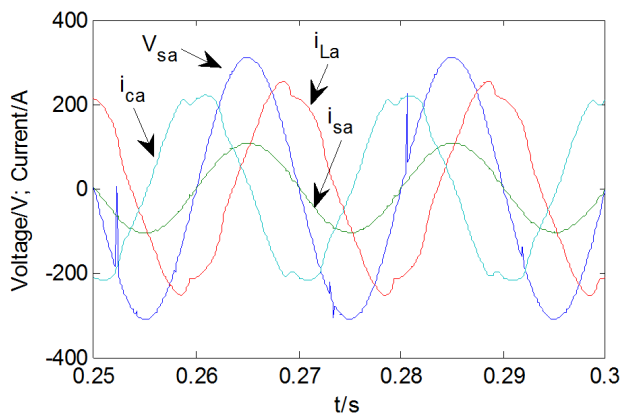
The steady-state performance waves of the system voltage, system current, load current, and device current were analyzed (Fig. 13). The dynamic performance of the control system is shown in Figs 14. The dynamic waves of the real-time, and reference q- and d-axis currents in the process of switching multiple loads are shown in Figs 15. Related simulation results show that the proposed modulation wave distribution algorithm fulfills the charging and discharging process that the automatic tracking control of the capacitors requires (Fig. 16).

#### 4.5. Experiment verification

The dynamic reactive compensation experiment device (i.e. the STATCOM) mainly comprises a control cabinet, several power cabinets, a starting cabinet, and a set of reactors. A cascaded structure, star-connection method, and H-bridge units are employed for a three-phase system design. The hardware structure of the control system includes the FPGA control circuit board, A/D circuit



(a) Steady-state performance of capacitive load

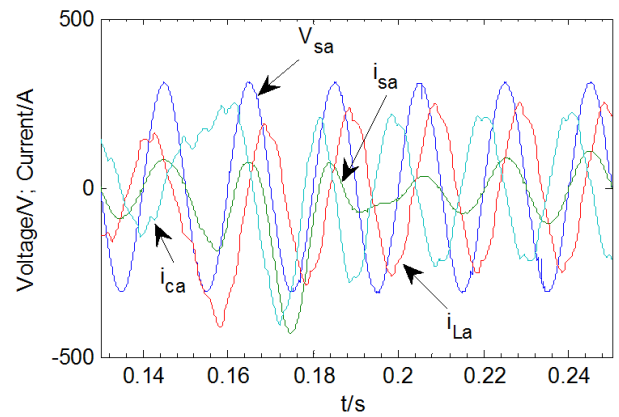


(b) Steady-state performance of inductive load

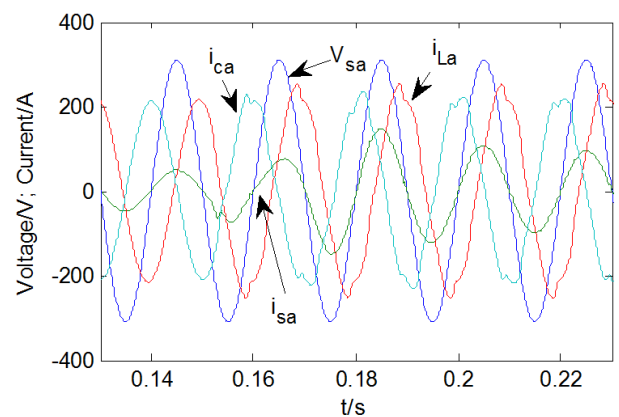
Figure 13: Steady-state performance waves of the capacitive and inductive loads compensation

boards, I/O circuit boards, optical fiber interface circuit boards, and the power circuit boards using multiple FPGA chips. The integral control principle diagram is shown in Fig. 17. The automatic control system of the programs in the FPGA fulfills the functions of sampling, operation of the phase-locked loop (PLL), sequencing of DC capacitor voltage, distribution strategy of the modulation wave and operation of the double-loop control algorithms.

The experimental results shown in Fig. 18 and Fig. 19 indicate that the experimental device can offer better compensation accuracy in steady-state or dynamic performance. The steady-state value of the load current is 150 A. The actual data indicate that the part of the reactive current which should be provided by the grid, is actually compensated by the STATCOM. The STATCOM therefore achieves dynamic current compensation without the need for any current from the grid. The results shown in Fig. 20 indicate that the proposed method has good harmonic currents tracking control ability. The real-time value of the DC-



(a) Dynamic performance of switching different loads



(b) Dynamic performance of sudden changes in load

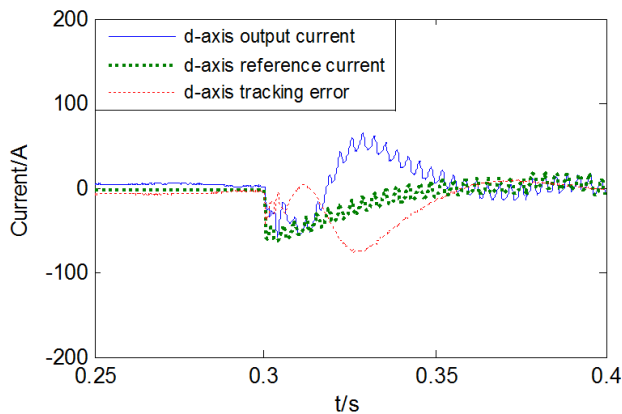
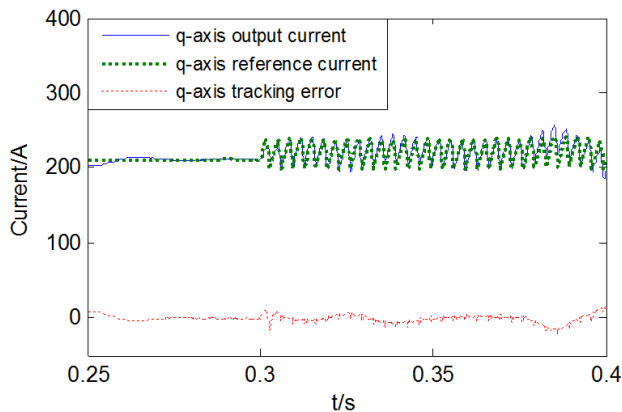
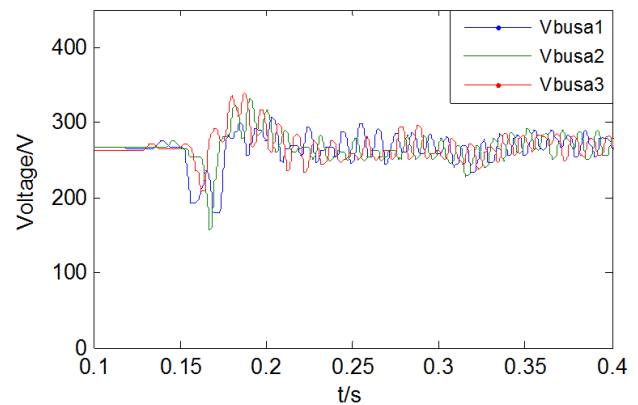
Figure 14: Dynamic performance waves of different loads

side capacitor voltage is shown in Fig. 21. Furthermore, the data indicate the balance control for the DC-side capacitor voltage.

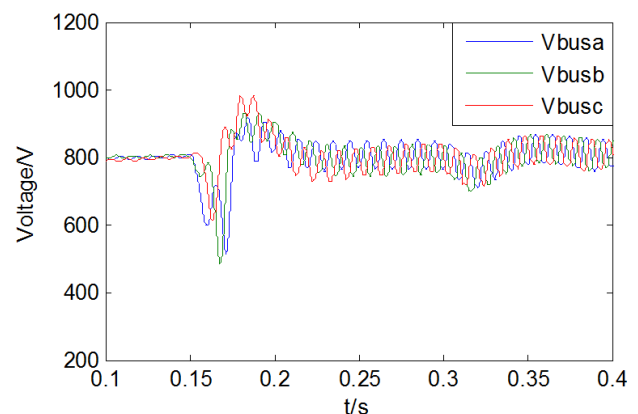
## 5. Conclusions

In this paper, a new STATCOM control strategy, employed as an efficient control scheme for fundamental and selective harmonic currents, was analyzed in detail from three angles. A new decoupling control method, a flexible comprehensive compensation scheme and special voltage balance control strategies were introduced to form the system control frameworks.

1. Due to a control problem with the state feedback decoupling method, the proposed control algorithm based on mathematical models of the STATCOM adopts an internal model decoupling controller to provide decoupled control of the d- and q-axis currents (i.e., the active and reactive currents).

(a) Current and tracking error waves of  $d$ -axis(b) Current and tracking error waves of  $q$ -axisFigure 15: Currents and tracking error of  $d$  and  $q$ -axis currents

(a) Balance control waves of each unit's voltage



(b) Balance control waves of phase-to-phase voltage

Figure 16: Balance control waves of DC-side capacitors

2. A new detection approach for the harmonic current, based on the  $d$ - $q$  synchronous reference frame and the DFT, was proposed and applied to complete the separate control of positive- and negative-sequence currents (i.e., the part of the harmonic current used for control).
3. The voltage imbalance problem of the DC-side capacitors was solved with an adaptive dynamic layered control scheme and modulation wave distribution strategies. Both the simulation and experimental results indicate that the comprehensive compensation current has a good dynamic and steady-state performance. Therefore, this control strategy should be of great value in engineering applications.

#### Acknowledgments

This work is supported by the Specialized Research Fund for the Doctoral Program of Higher Education of China, grant 20110095110014.

#### References

- [1] Z. Yao, Q. Zhao, X. Liu, Research on grid-connected technology of inverter based on quasi synchronous principle, *Power System Protection and Control* 39 (24) (2011) 123–126.
- [2] B. Singh, R. Saha, A. Chandra, K. Al-Haddad, Static synchronous compensators (statcom): a review, *Power Electronics, IET* 2 (4) (2009) 297–324.
- [3] L. Fei, D. Shanxu, Z. Xiaoming, et al., Design of two loop controller in grid-connected inverter with  $l_{cl}$  filter, *Proceedings of the CSEE* 29 (S1) (2009) 234–240.
- [4] D. Zhang, Z. Qiu, Y. Li, Shunt active power filter with high steady-state performance based on  $l_{cl}$ -filter, *Transactions of China Electrotechnical Society* 29 (12) (2009) 234–240.
- [5] X. Zhang, W. Shao, S. Yang, Multi-loop control scheme of a grid side converter with LCL-filter, *Journal of HeFei University of Technology* 32 (7) (2005) 72–76.
- [6] Z. Xianping, L. Zixu, L. Yaxi, et al., A novel control strategy for pwm rectifier with  $l_{cl}$  filter, *Transactions of China Electrotechnical Society* 22 (2) (2007) 74–77.
- [7] S. Leskover, M. Marchesini, *Power Electronics and Application (EPE)*, European Power Electronics Association, Germany, 2005, Ch. Control techniques for DC-link voltage ripple minimization in cascaded multilevel converter structures, pp. 23–32.
- [8] W. Wenhui, L. Wenhua, S. Qiang, et al., Research on fast dynamic control of static synchronous compensator using cascade

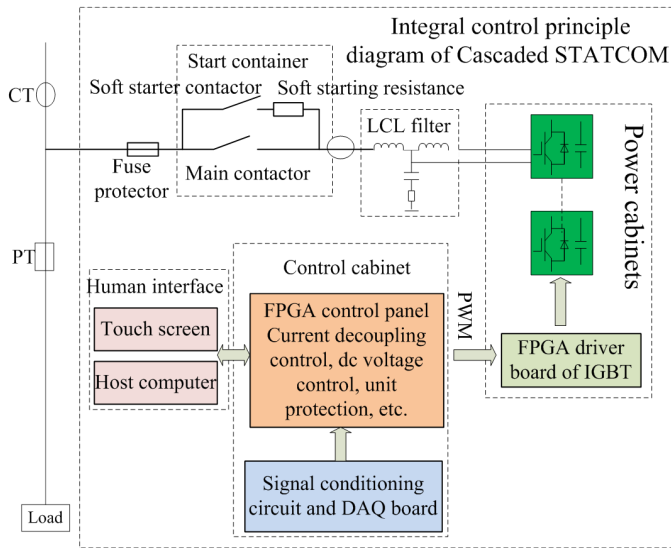


Figure 17: Structure diagram of controller

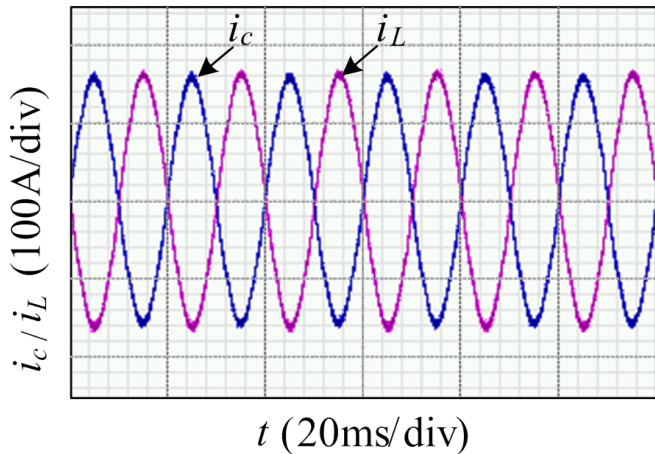


Figure 18: Steady-state compensation performance

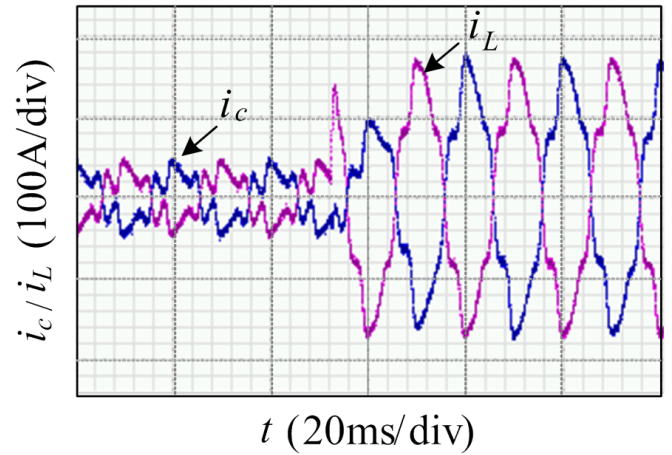


Figure 19: Dynamic compensation performance

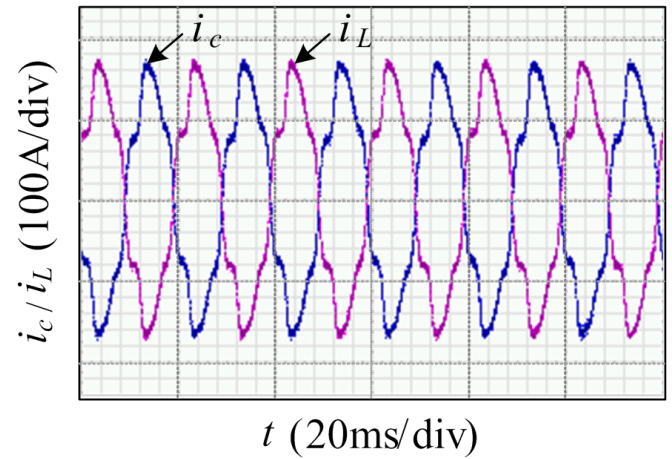


Figure 20: Waves of harmonics compensation

multilevel inverters, Proceedings of the CSEE 25 (3) (2005) 23–28.

- [9] M. Liserre, R. Teodorescu, F. Blaabjerg, Multiple harmonics control for three-phase grid converter systems with the use of pi-res current controller in a rotating frame, Power Electronics, IEEE Transactions on 21 (3) (2006) 836–841.
- [10] L. Chunxi, M. Weiming, S. Chi, et al., Design of output lc filter and low order harmonics suppression in high power 400hz inverter, Transactions of China Electrotechnical Society 26 (6) (2011) 129–136.
- [11] K. Sozanski, Sliding dft control algorithm for three-phase active power filter, in: Applied Power Electronics Conference and Exposition, 2006. APEC'06. Twenty-First Annual IEEE, IEEE, 2006, pp. 7–pp.
- [12] Y. Li, W. Lu, X. Peng, M. GUO, Dc voltage measurement and control for cascaded statcom, Proceedings of the CSEE 3 (2011) 005.
- [13] W.-h. LIU, Q. SONG, L.-t. TENG, W. WANG, W.-h. WEI, J.-c. GENG, Balancing control of dc voltages of 50mva statcom based on cascade multilevel inverters [j], Proceedings of the Csee 4.

- [14] M. Ren, Y. Sun, Voltage balance control of dc capacitors of 11-level cascade statcom, Automation of Electric Power Systems 4 (6).
- [15] H. Yinghong, R. Jiajia, W. Jianze, et al., Balancing control method of dc voltage of cascaded h-bridge statcom, Electric Machines and Control 14 (11) (2010) 31–36.

Real-time value of capacitor voltage and temperature						
Detail	Capacitor voltage value (V)			Temperature monitoring ( $^{\circ}\text{C}$ )		
No.	A	B	C	A	B	C
1	837	837	813	46	42	48
2	838	818	813	46	41	44
3	833	888	841	44	48	46
4	814	838	819	44	42	44
5	824	823	851	44	44	42
6	833	848	897	44	42	44
7	821	843	821	46	44	46
8	889	823	821	46	46	44

Figure 21: Real-time capacitor voltage value